Applying Virial theorem in continuous potential of two scales

Ney M. Barraz Jr. and Marcia C. Barbosa*

Instituto de Fsica, Universidade Federal do Rio Grande do Sul
Caixa Postal 15051, CEP 91501-970
Porto Alegre, RS, Brazil
**marcia.barbosa@ufrgs.br*

In this paper we study the pressure-pressure phase diagram of a family of core-softened continuous potentials characterized by two length scales. The first scale is a repulsive core with a softening region and the second scale is an attractive well. Three different distances between the two length scales are checked for the presence of density, diffusion and structural anomalies. We found that in this model the critical point goes to negative pressures as the distance between the two length scales is above a certain threshold. This result is explained in the framework of the virial expression for the pressure.

1. Introduction

Most liquids contract upon cooling. This is not the case of water, a liquid where the specific volume at ambient pressure starts to increase when cooled below $T = 4^oC$.[1] Besides, in a certain range of pressures, also exhibits an anomalous increase of compressibility and specific heat upon cooling.[2,3] It is less well known that water diffuses faster under pressure at very high densities and at very low temperatures.[2,4–6]

These anomalies are proposed to be related to a second critical point between two liquid phases, a low density liquid (LDL) and a high density liquid (HDL).[7] This critical point was discovered by computer simulations. This work suggests that this critical point is located at the supercooled region beyond the line of homogeneous nucleation and thus cannot be experimentally measured. Even if this limitation, this hypothesis has been supported by experimental results.[8–11]

Spherical symmetric models became the simplest framework to understand the physics of the liquid-liquid phase transition and liquid state anomalies. Acknowledging that core softened (CS) potentials may engender a demuxing transition between two liquids of different densities, a number of CS potentials were proposed to model the anisotropic systems described

above. They possess a repulsive core that exhibits a region of softening where the slope changes dramatically. This region can be a discontinuous[12–23] or a continuous[24–38] shoulder or a ramp.[11,16,37–43]

These models show two liquid phases if the attractive part of the potential is deep enough and density, diffusion and structural anomalies if the two length scales would be accessible.[44,45] In the cases in which the second critical point is present, the maximum pressure of the temperature of maximum density line does not exceed the critical pressure.[44–46] However, in many CS potentials in which an attractive part is present the liquid-liquid phase transition is located in an nonphysical region of the pressure temperature phase diagram,[44,45] namely at negative pressures. In these potentials the TMD line is also located at negative pressures and, therefore, experimentally inaccessible. Unfortunately no simple theory can predict if a given CS potential has a liquid-liquid critical at positive pressures or not.

Here we propose a simple prescription that indicates without the need of performing the simulations if a CS potential has a first and a second critical points with positive pressures. This recipe is tested for three different CS potentials characterized by two length scales: a repulsive shoulder and an attractive well. In order to vary only the pressure of the second critical point, keeping the temperature constant, the potentials chosen for testing our prescription have the same energy difference between the two length scales.

The remaining of this paper goes as follows. In Sec. 1.1 the three models are introduced. The simulations details are given Sec. 1.2. In Sec. 1.3 presents the Virial theorem. The pressure-temperature phase diagrams, density, diffusion and structural anomalous are presented in Sec. 2. At the end of this section a prescription for the presence of a second critical point at positive pressures is proposed and tested in the three models. Finally, Sec. 3 presents the conclusion.

1.1. *The Model*

We consider a system of N particles, with diameter σ, where the pair interaction is described by a family of continuous potentials given by

$$U(r) = \epsilon \left[\left(\frac{\sigma}{r}\right)^a - \left(\frac{\sigma}{r}\right)^b \right] + \sum_{j=1}^{4} h_j \exp\left[-\left(\frac{r - c_j}{w_j}\right)^2 \right] \quad . \tag{1}$$

The first term is Lennard-Jones-like potential and the second parcel contains four Gaussians centered in c_j with $j = 1, 2, 3, 4$.

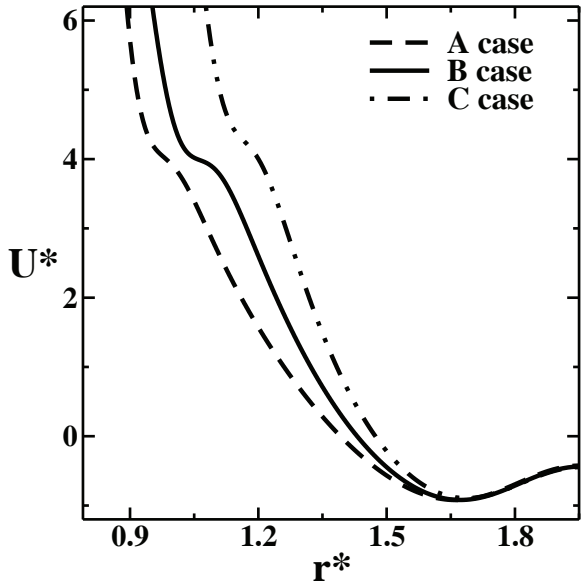

Fig. 1. Interaction potential obtained by changing parameters c_1 and h_1 in the Eq. (1). The potential and the distances are in dimensionless units $U^* = U/\gamma$ and $r^* = r/r_0$.

In this paper we analyze three different potentials, A, B and C, illustrated in Fig. 1 with $U^* = U/\gamma$ and $r^* = r/r_0$. They are obtained using three different values for c_1, c_2, w_1, h_1 and h_2 as shown in the Table 1. The remaining parameters of Eq. (1) together with the reference values, c_1^{ref}, c_2^{ref}, w_1^{ref}, h_1^{ref} and h_2^{ref} are fixed and are given in units of energy, γ, and length, r_0, in the Table 2.

Our potentials, shown in Fig. 2, exhibit a shoulder scale and an attractive scale what characterizes systems with thermodynamic, dynamic and structural anomalous behavior. In all the three cases, the difference between the potential energy of the shoulder scale and the attractive scale is kept fixed while the distance between the two scales is varied. Thus, the distance between the two length scales is for the A case: $d_A = 0.70$; for the B case: $d_B = 0.60$; and for the C case: $d_C = 0.50$; in units of r_0. By fixing the potential energy difference we expect to have all the three cases the temperature of the second critical point about the same value[44,45,47] but with very different pressures. Therefore, we have chosen this set of potentials for testing our prescription for the presence or not of second critical point.

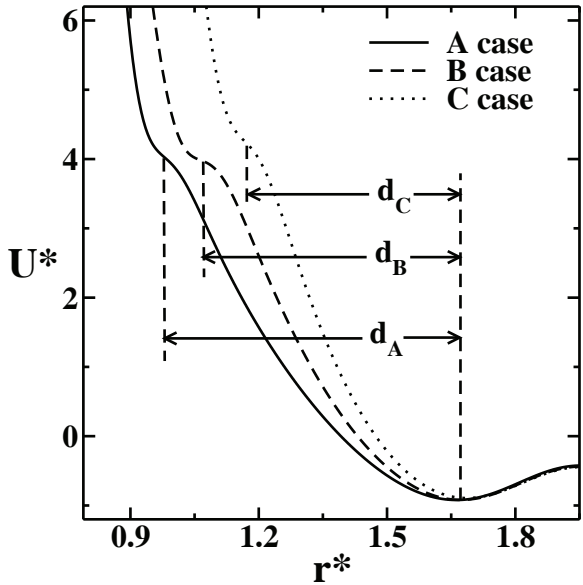

Fig. 2. The distance between the two scales are: $d_A = 0.70$, $d_B = 0.60$ and $d_B = 0.50$.

1.2. *Details of Simulations*

The properties of the system were obtained by NVT molecular dynamics using Nose-Hoover heat-bath with coupling parameter $Q = 2$. The system is characterized by 500 particles in a cubic box with periodic boundary conditions, interacting with the intermolecular potential described above. All physical quantities are expressed in reduced units.

Standard periodic boundary conditions together with predictor-corrector algorithm were used to integrate the equations of motion with a time step $\Delta t^* = 0.002$ and potential cut off radius $r_c^* = 3.5$. The initial configuration is set on solid or liquid state and, in both cases, the equilibrium state was reached after $t_{eq}^* = 1000$. From this time on the physical quantities were stored in intervals of $\Delta t_R^* = 1$ during $t_R^* = 1000$. The system is uncorrelated after $t_d^* = 10$, from the velocity auto-correlation function, and 50 decorrelated samples were used to get the average of the physical quantities. The thermodynamic stability of the system was checked analyzing the dependence of pressure on density, by the behavior of the energy and also by visual analysis of the final structure, searching for cavitation.

All the thermodynamic, dynamic and structural physical quantities are given in terms of dimensionless units of γ and r_0 listed in Table 2.

Table 1. Parameters c_1, c_2, w_1, h_1 and h_2 for potentials A, B and C.

Potential	c_1	c_2	w_1	h_1	h_2
A	$0.90\, c_1^{ref}$	$1.27\, c_2^{ref}$	$0.98\, w_1^{ref}$	$0.64\, h_1^{ref}$	$0.45\, h_2^{ref}$
B	$1.00\, c_1^{ref}$	$1.00\, c_2^{ref}$	$1.00\, w_1^{ref}$	$0.50\, h_1^{ref}$	$1.00\, h_2^{ref}$
C	$1.10\, c_1^{ref}$	$0.73\, c_2^{ref}$	$1.00\, w_1^{ref}$	$0.65\, h_1^{ref}$	$2.70\, h_2^{ref}$

Table 2. Parameters for potentials A, B and C in units of Å and of $kcal/mol$.

Parameter	Value	Parameter	Value	Parameter	Value
a	9.056	w_1^{ref}	0.253	h_3	-0.451
b	4.044	w_2	1.767	h_4	0.230
ϵ	0.006	w_3	2.363	c_1^{ref}	2.849
σ	4.218	w_4	0.614	c_2^{ref}	1.514
r_0	2.860	h_1^{ref}	-1.137	c_3	4.569
γ	50.00	h_2^{ref}	3.626	c_4	5.518

The diffusion coefficient is obtained from the expression

$$D = \lim_{t\to\infty} \frac{\left\langle \left[\vec{r}_j\left(t_0+t\right) - \vec{r}_j\left(t_0\right)\right]^2 \right\rangle_{t_0}}{6t,} \tag{2}$$

where $\vec{r}_j\left(t\right)$ are the coordinates of particle j at time t and $\langle\cdots\rangle_{t_0}$ denotes an average over all particles and over all t_0.

1.3. *Virial Theorem*

Do the potentials A, B and C have a liquid-liquid critical point? Before computing the pressure-temperature phase diagram for these three potentials, we propose that this question can be answer on basis of the response function and virial expression for the pressure.

The pressure can be computed from the expression[48]

$$\frac{6p}{\rho} = \left(6k_BT + \Psi\right) \tag{3}$$

where Ψ is the Virial given by $\Psi = N\left\langle \vec{r}_{ij}\cdot\vec{F}_{ij}\right\rangle$, the braket denotes thermodynamic averaging. Since $\vec{r}_{ij} = \vec{r}_i - \vec{r}_j$, $\vec{F}_{ij}$ the force on molecule i due to j.

The isothermal compressibility is defined as

$$K_T \equiv -\frac{1}{V}\left(\frac{\partial V}{\partial p}\right)_T = \frac{1}{\rho}\left(\frac{\partial \rho}{\partial p}\right)_T . \tag{4}$$

K_T is thus response of the volume to its conjugate variable pressure and it is proportional to fluctuations in specific density, $K_T \propto \left\langle (\delta\rho)^2 \right\rangle$. Using Eq. (3) the isothermal compressibility can be written as:

$$K_T = \frac{6}{\rho^2\left(\frac{6p}{\rho^2} + \frac{\partial \Psi}{\partial \rho}|_{N,T}\right)} . \tag{5}$$

The condition $K_T < 0$ implies the lost of stability and consequently the phase separation. For positive pressure ($p > 0$) the stability is lost for:

$$\frac{6p}{\rho^2} < -\left(\frac{\partial \Psi}{\partial \rho}\right)_{T,N} . \tag{6}$$

Using Eq. (3) and taking into account that the temperature is positive, the above inequality leads to the expression:

$$\frac{\Psi}{\rho} < -\left(\frac{\partial \Psi}{\partial \rho}\right)_{T,N} \tag{7}$$

For simplicity let us define the following quantities:

$$f_1 = -\left(\frac{\partial \Psi}{\partial \rho}\right)_{T,N} , \tag{8}$$

$$f_2 = \frac{\rho}{2}\left(\frac{\partial^2 \Psi}{\partial \rho^2}\right)_{T,N} , \tag{9}$$

$$f_3 = \left(\frac{\Psi}{\rho}\right)_{T,N} . \tag{10}$$

From the lost of stability condition, Eq. (7), Eq. (8) and Eq. (9) follows

$$f_3 < f_1 . \tag{11}$$

This expression together with the condition for positive pressure and positive temperature arises:

$$f_3 > 0 ,$$

$$f_1 > 0 . \tag{12}$$

Table 3. Critical point and density location for potentials A, B, C, and D.

Potential	T^*_{c1}	p^*_{c1}	ρ^*_{c1}
A	2.42	0.11	$0.10 \leq \rho^*_{c1} \leq 0.13$
B	1.98	0.08	$0.10 \leq \rho^*_{c1} \leq 0.13$
C	1.58	0.50	$0.10 \leq \rho^*_{c1} \leq 0.13$
Potential	T^*_{c2}	p^*_{c2}	ρ^*_{c2}
A	0.57	-0.24	$0.56 \leq \rho^*_{c2} \leq 0.70$
B	0.47	1.83	$0.54 \leq \rho^*_{c2} \leq 0.68$
C	0.30	7.10	$0.53 \leq \rho^*_{c2} \leq 0.58$

At the critical point the first and second derivatives of the pressure given by Eq. (3) with respect to the density are zero, namely:

$$\left(\frac{\partial p}{\partial \rho}\right)_T = 0, \tag{13}$$

$$\left(\frac{\partial^2 p}{\partial \rho^2}\right)_T = 0. \tag{14}$$

what implies that f_2 changes sign across the criticality.

2. Results and Discussion

2.1. *Pressure-Temperature Phase Diagram*

Fig. 3 illustrates the pressure-temperature phase diagram for the potentials A, B and C. The system at high temperatures has a fluid phase and a gas phase (not shown) forming a first order line ending at a first critical point. The values of pressure, temperature and density region of the critical point is located in the pressure-temperature phase diagram are listed in Sec. 3.

2.2. *Density Anomaly*

From the Maxwell relation,

$$\left(\frac{\partial V}{\partial T}\right)_p = -\left(\frac{\partial p}{\partial T}\right)_V \left(\frac{\partial V}{\partial p}\right)_T, \tag{15}$$

the maximum in $\rho\,(T)$ versus temperature at constant pressure given by $(\partial\rho/\partial T)_p = 0$ is equivalent to the minimum of the pressure versus temperature at constant density, namely

$$\left(\frac{\partial p}{\partial T}\right)_\rho = 0, \tag{16}$$

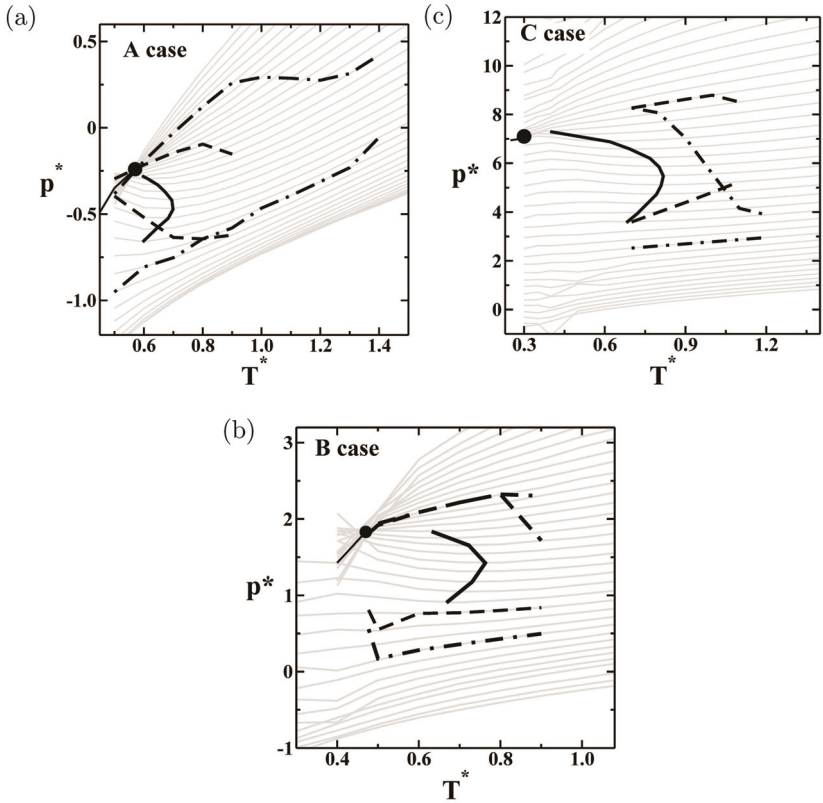

Fig. 3. Pressure-temperature phase diagram for A potential in the left-hand side, for B potential in the middle and for C potential in the right-hand side. The thin grey lines are the isochores $0.30 < \rho^* < 0.65$. The liquid-liquid critical point is the dot, the temperature of maximum density is the solid thick line, the diffusion extrema is the dashed line and the structural extrema is the dashed-dotted line.

$$\left(\frac{\partial^2 p}{\partial T^2}\right)_\rho > 0. \tag{17}$$

The three system exhibit a region in the pressure and temperature in which as the temperature is decreased the density decreases at constant pressure. The temperature in maximum density (TMD) is illustrated as solid lines in the Fig. 3. The density ranges of the TMD are: A case $0.48 \leq \rho^* \leq 0.56$; B case $0.46 \leq \rho^* \leq 0.54$; and C case $0.44 \leq \rho^* \leq 0.55$.

This result can be understood using the radial distribution function. The TMD is related to the presence of large regions in the system in which par-

ticles are in two preferential distances represented by the first- and second-scale represented by the two first peaks in the radial distribution function in our potential.[33,49–51] As the temperature is increased the percentage of particles in closest scales decreases. The decrease of particles in the first scale leads to a decrease of density with the increase of temperature. Fig. 4, as the temperature is increased the percentage of particles at the closest distance increases while the percentage of particles in the second scale decreases. The increase of particles in the first scale leads to an increase of density with temperature what characterizes the anomalous region. The density anomaly is, therefore, related to the increase of the probability of particles to be in the first scale when the temperature is increased while the percentage of particles in the second-scale decreases.

Fig. 5 compares the TMD and the critical points for the three potentials. The increase in the slope between the two length scales makes harder to the high density liquid to be formed, requiring higher pressure. In addition it also makes the fluid phase more stable and therefore the two critical points move to lower temperatures. The density anomalous region that represents the range in temperature and pressures in which the scales compete also increases with the decrease of the distance between the two length scales.

2.3. *Diffusion Anomaly*

Fig. 6 shows the behavior of the dimensionless diffusion coefficient, D^*, as function of the dimensionless density, ρ^*, at constant temperature for the three cases. The solid lines are a polynomial fits to the data obtained by simulation (the dots in the Fig. 6). For normal liquids, the diffusion at constant temperature increases with the decrease in the density. For potentials A, B, and C the diffusion has a region in the pressure-temperature phase diagram in which the diffusion increases with density. This is the diffusion anomalous region. In Fig. 6 one dashed line joints the points of the density (or pressure) of minimum diffusion for different temperatures and another dashed line links the points of density (or pressure) of maximum diffusion for different temperatures.

2.4. *Structural Anomaly*

The translational order parameter is defined as[5,52,53]

$$t = \int_0^{\xi_c} |g(\xi) - 1| d\xi, \tag{18}$$

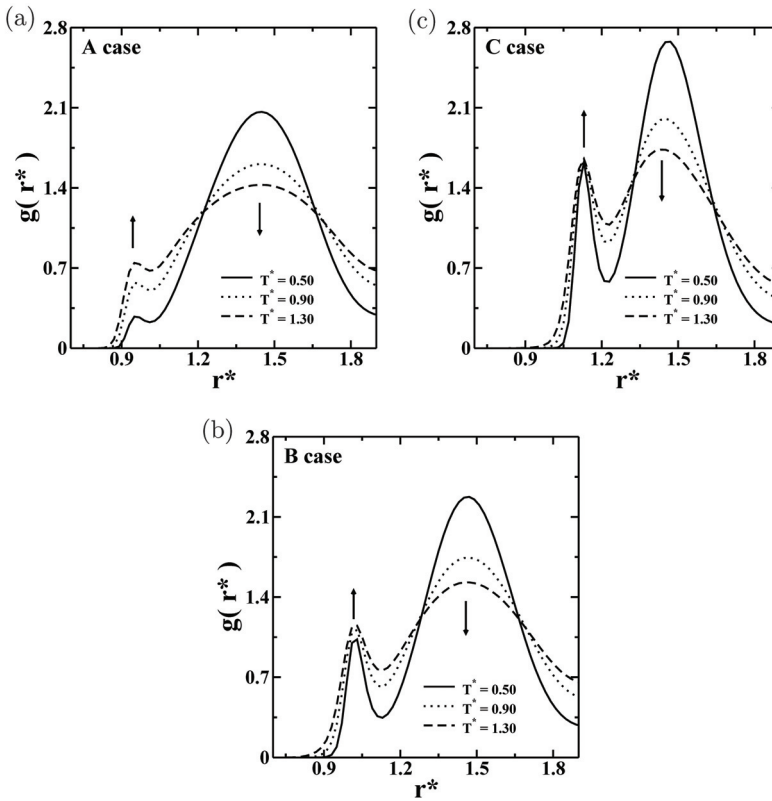

Fig. 4. Radial distribution function obtained using NVT simulations versus distance for A, B and C cases, with density fixed ($\rho = 0.50$). The arrows indicate the direction of increasing temperature.

where $\xi = r\rho^{1/3}$ is the distance r in units of the mean interparticle separation $\rho^{-1/3}$, ξ_c is the cutoff distance set to half of the simulation box times[29] $\rho^{-1/3}$, and $g(\xi)$ is the radial distribution function proportional to the probability of finding a particle at a distance ξ from a referent particle. The translational order parameter measure how structured is the system. For an ideal gas $g = 1$ and $t = 0$, and the case of crystal phase $g \neq 1$ over long distances and t is large. Therefore for normal fluids t increases with the increase in the density.

Fig. 7 shows the translational order parameter as a function of the density for fixed temperatures. The dots represent the simulation data and the solid line the polynomial fit to the data. For potentials A, B, and C

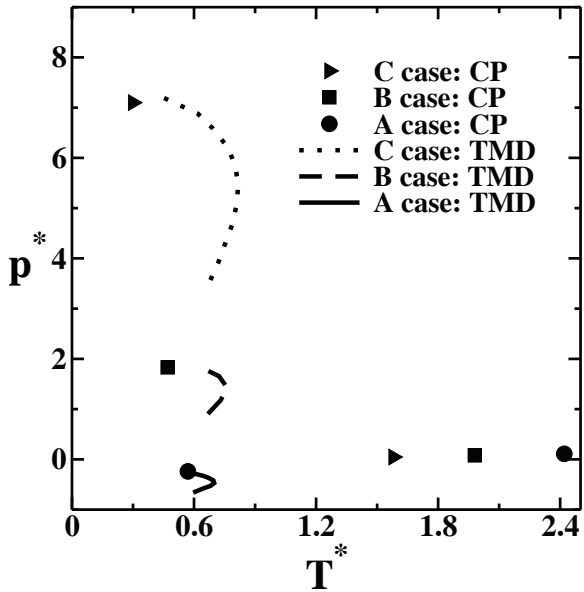

Fig. 5. Comparison between the range of the TMD lines in the pressure-temperature phase diagram for the three systems.

there is a region of densities in which the translational parameter decreases as the density increases. A dotted-dashed line illustrates the region of local maximum of t^* and minimum of t^* limiting the anomalous region.

2.5. *Critical Point*

In the previous chapter we suggested that the presence of phase boundary between two phases appears if

(1) $f_1 > 0$, $f_3 > 0$
(2) $f_1 > f_3$
(3) f_2 changes signed

Here we test these three conditions in our potentials A, B and C. Fig. 8 shows the curves f_1, f_2 and f_3 versus density for all potentials, where $f_{1,2,3}$ are given by Eq. (8), Eq. (9) and Eq. (10).

The curves f_1 and f_3 are positive, $f_1 > f_3$ and f_2 changes sign for the densities located at the liquid-gas phase boundary, namely $\rho^* \approx 0.13$. Therefore, $f_{1,2,3}$ satisfy the conditions instability close to the liquid-gas critical point.

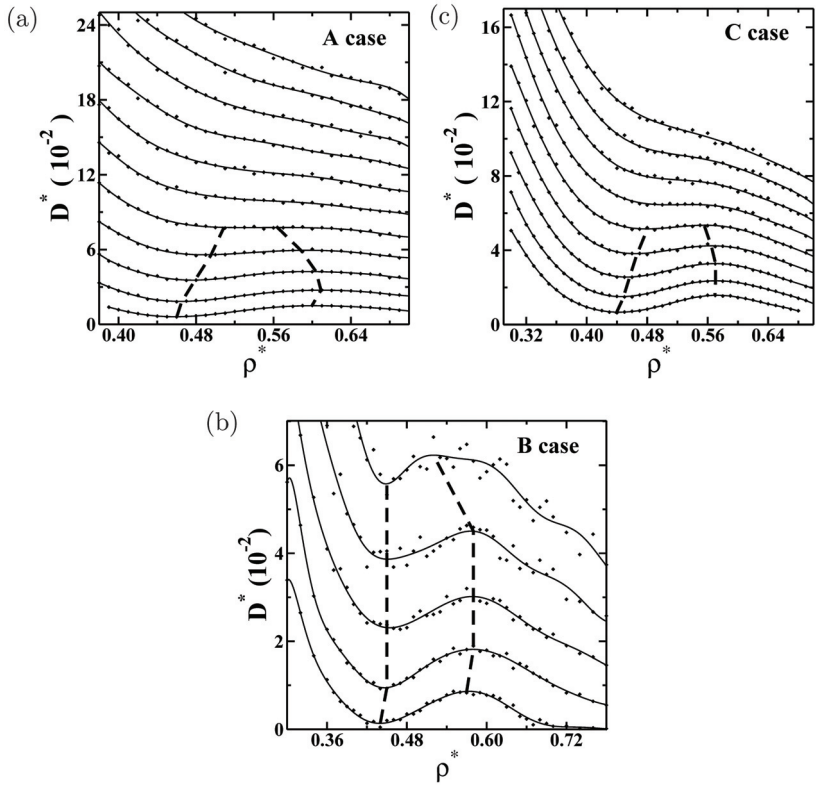

Fig. 6. Diffusion coefficient as a function of density. The dots are the simulational data and the solid lines are polynomial fits. The dashed lines connect the densities of minima and maxima diffusivity that limit the diffusion anomalous region.

For higher densities, the three conditions are also obeyed for potentials B and C close to the liquid-liquid coexistence at $\rho^* \approx 0.68$ for potential B and $\rho^* \approx 0.58$ for potential C. For the potential A, however the conditions were not satisfies what is in agreement with the absence of liquid-liquid critical point at positive pressures. In the case of potential A criticality appears at negative pressures.

3. Conclusions

In this article, we constructed the pressure-temperature phase diagram of a two length scale family of potentials. These core-softened potentials are built to reproduce the anomalies present in water. The three families differ

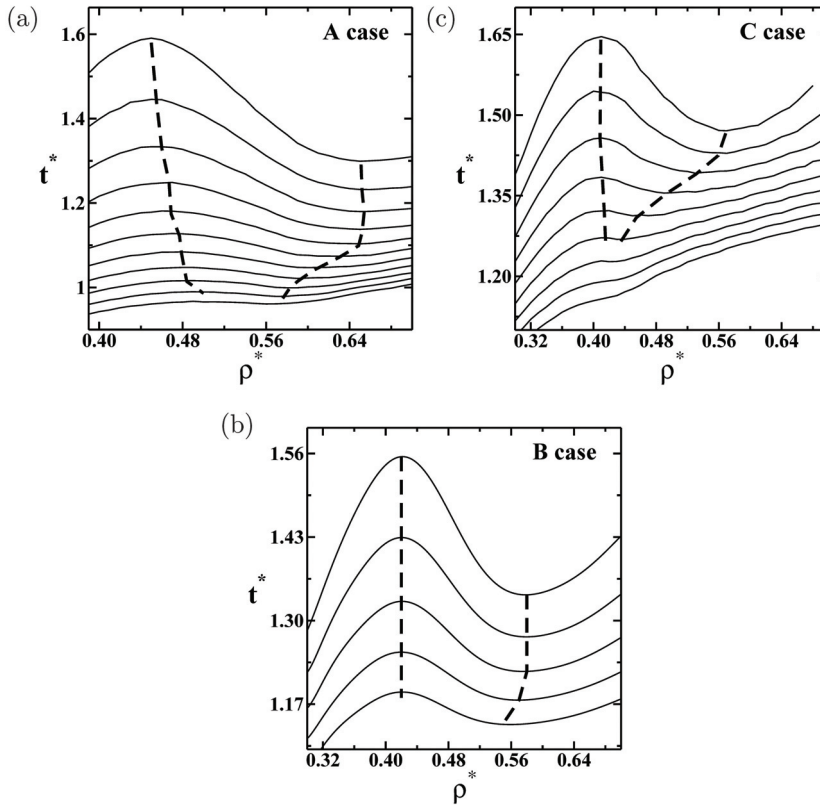

Fig. 7. The translational order parameter as a function of density for fixed temperatures: $T^* = 1.10, 1.00, 0.90, 0.80, 0.70$, and 0.60 from top to bottom. The dot-dashed lines locate the density of maxima and minima t^*.

by the distance between the two scales. We analyze the effect of decreasing the distance between the two scales in the location in the pressure-temperature phase diagram of the density, diffusion and structural anomalies. In addition we explore whether the decrease of the distance scales shifts the critical point and the temperature of maximum density for a region of positive pressures. We found that the anomalies and liquid-liquid critical point move to positive results containing a low temperature variation in the measure that the shoulder is close to the attractive part. This indicates that the probability of the particles migrate from one scale to another increases with the closeness of the two scales. As the shoulder is close to the attractive part, are more particles in this range compared to other larger

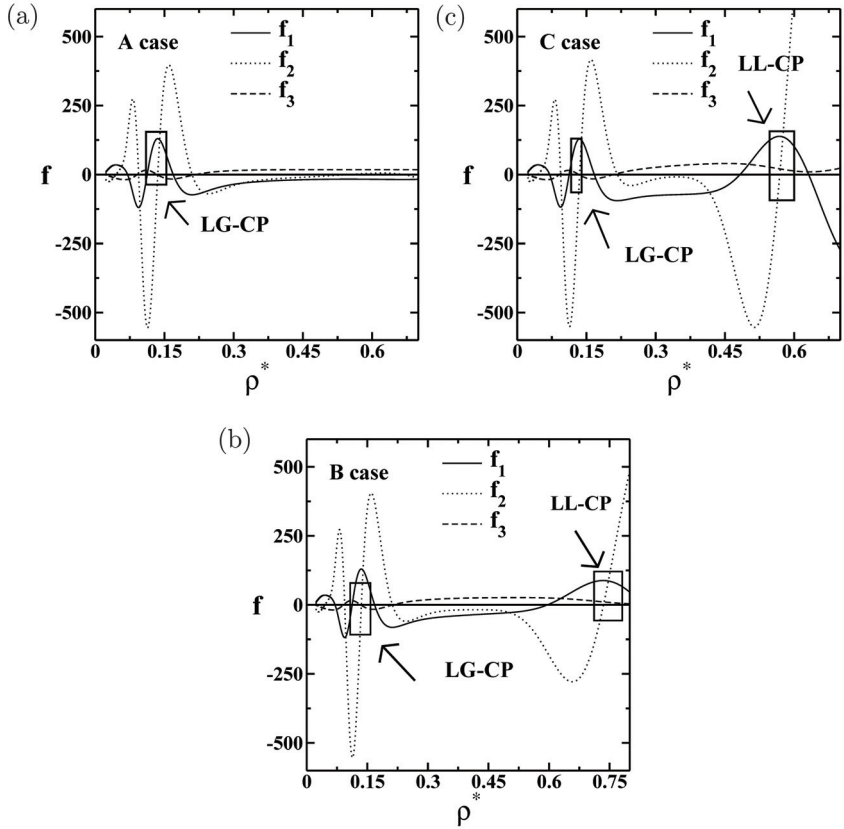

Fig. 8. f_1, f_2 and f_3 versus resuced density for the three potentials. The squares and arrows illustrate the regions where the conditions $f_1 > f_3$, $f_3 > 0$ and f_2 changing signs indicates criticality.

distances between the two scales. Finally we propose a simple condition that involves the different derivatives of the potential to predict if the critical point occurs at positive pressures. This condition was confirmed with our results obtained for the three potentials.

Acknowledgements

We thank for financial support the Brazilian science agencies CNPq and Capes. This work is partially supported by CNPq, INCT-FCx.

References

1. R. Waler, *Essays of Natural Experiments* (Johnson Reprint, New York, 1964).
2. F. X. Prielmeier, E. W. Lang, R. J. Speedy and H.-D. Lüdemann, *Phys. Rev. Lett.* **59**, 1128 (1987).
3. L. Haar, J. S. Gallangher and G. Kell, *NBS/NRC Steam Tables. Thermodynamic and Transport Properties and Computer Programs for Vapor and Liquid States of Water in SI Units.*, 1st edn. (Hemisphere Publishing Co., Washington D.C., 1984).
4. C. A. Angell, E. D. Finch and P. Bach, *J. Chem. Phys.* **65**, 3063 (1976).
5. J. R. Errington and P. G. Debenedetti, *Nature* **409**, 318 (2001).
6. P. A. Netz, F. W. Starr, H. E. Stanley and M. C. Barbosa, *J. Chem. Phys.* **115**, 344 (2001).
7. P. H. Poole, F. Sciortino, U. Essmann and H. E. Stanley, *Nature* **360**, 324 (1992).
8. O. Mishima and H. E. Stanley, *Nature* **396**, 329 (1998).
9. S. H. Chen, F. Mallamace, C. Y. Mou, M. Broccio, C. Corsaro, A. Faraone and L. Liu, *Proc. Natl. Acad. Sci. USA* **103**, 12974 (2006).
10. L. Liu, S.-H. Chen, A. Faraone, S.-W. Yen and C.-Y. Mou, *Phys. Rev. Lett.* **95**, 117802 (2005).
11. L. Xu, P. Kumar, S. V. Buldyrev, S.-H. Chen, P. Poole, F. Sciortino and H. E. Stanley, *Proc. Natl. Acad. Sci. USA* **102**, 16558 (2005).
12. G. Franzese, M. I. Marques and H. E. Stanley, *Phys. Rev. E* **67**, 011103 (2003).
13. A. Balladares and M. C. Barbosa, *J. Phys.: Condens. Matter* **16**, 8811 (2004).
14. V. B. Henriques and M. C. Barbosa, *Phys. Rev. E* **71**, 031504 (2005).
15. V. B. Henriques, N. Guissoni, M. A. Barbosa, M. Thielo and M. C. Barbosa, *Mol. Phys.* **103**, 3001 (2005).
16. P. C. Hemmer and G. Stell, *Phys. Rev. Lett.* **24**, 1284 (1970).
17. M. Pretti and C. Buzano, *J. Chem. Phys.* **121**, 11856 (2004).
18. S. V. Buldyrev, P. Kumar, P. G. Debenedetti, P. J. Rossky and H. E. Stanley, *Proc. Natl. Acad. Sci. USA* **104**, 20177 (2007).
19. N. G. Almarza, J. A. Capitan, J. A. Cuesta and E. Lomba, *J. Chem. Phys.* **131**, 124506 (2009).
20. E. Lomba, N. G. Almarza, C. Martin and C. McBride, *J. Chem. Phys.* **126**, 244510 (2007).
21. D. Y. Fomin, , N. V. Gribova, V. N. Ryzhov, S. M. Stishov and D. Frenkel, *J. Chem. Phys.* **129**, 064512 (2008).
22. N. V. Gribova, Y. D. Fomin, D. Frenkel and V. N. Ryzhov, *Phys. Rev. E* **79**, 051202 (2009).
23. A. B. de Oliveira and M. C. Barbosa, *J. Phys.: Condens. Matter* **17**, 399 (2005).
24. H. M. Gibson and N. B. Wilding, *Phys. Rev. E* **73**, 061507 (2006).
25. G. Franzese, G. Malescio, A. Skibinsky, S. V. Buldyrev and H. E. Stanley, *Nature* **409**, 692 (2001).
26. A. Skibinsky, S. V. Buldyrev, G. Franzese, G. Malescio and H. E. Stanley, *Phys. Rev. E* **69**, 061206 (2005).

27. G. Franzese, G. Malescio, A. Skibinsky, S. V. Buldyrev and H. E. Stanley, *Phys. Rev. E* **66**, 051206 (2002).
28. A. B. de Oliveira, P. A. Netz, T. Colla and M. C. Barbosa, *J. Chem. Phys.* **124**, 084505 (2006).
29. A. B. de Oliveira, P. A. Netz, T. Colla and M. C. Barbosa, *J. Chem. Phys.* **125**, 124503 (2006).
30. A. B. de Oliveira, M. C. Barbosa and P. A. Netz, *Physica A* **386**, 744 (2007).
31. A. B. de Oliveira, P. A. Netz and M. C. Barbosa, *Eur. Phys. J. B* **64**, 48 (2008).
32. A. B. de Oliveira, G. Franzese, P. A. Netz and M. C. Barbosa, *J. Chem. Phys.* **128**, 064901 (2008).
33. A. B. de Oliveira, P. A. Netz and M. C. Barbosa, *Europhys. Lett.* **85**, 36001 (2009).
34. P. Vilaseca and G. Franzese, *J. Non-Cryst. Solids* **357**, 419 (2011).
35. A. Scala, M. R. Sadr-Lahijany, N. Giovambattista, S. V. Buldyrev and H. E. Stanley, *J. Stat. Phys.* **100**, 97 (2000).
36. P. Camp, *Phys. Rev. E* **71**, 031507 (2005).
37. P. Camp, *Phys. Rev. E* **68**, 061506 (2003).
38. N. B. Wilding and J. E. Magee, *Phys. Rev. E* **66**, 031509 (2002).
39. E. A. Jagla, *J. Chem. Phys.* **110**, 451 (1999).
40. E. A. Jagla, *J. Chem. Phys.* **111**, 8980 (1999).
41. S. Maruyama, K. Wakabayashi and M. Oguni, *AIP Conf. Proc.* **708**, 675 (2004).
42. R. Kurita and H. Tanaka, *Science* **206**, 845 (2004).
43. Z. Yan, S. V. Buldyrev, P. Kumar, N. Giovambattista, P. G. Debenedetti and H. E. Stanley, *Phys. Rev. E* **76**, p. 051201 (2007).
44. N. M. Barraz Jr., E. Salcedo and M. C. Barbosa, *J. Chem. Phys.* **131**, 094504 (2009).
45. J. da Silva, E. Salcedo, A. B. Oliveira and M. C. Barbosa, *J. Phys. Chem.* **133**, 244506 (2010).
46. E. Salcedo, A. B. de Oliveira, N. M. B. Jr., C. Chakravarty and M. C. Barbosa, *J. Chem. Phys.* **135**, 044517 (2011).
47. Z. Y. Yan, S. V. Buldyrev, P. Kumar, N. Giovambattista and H. E. Stanley, *Phys. Rev. E* **77**, 042201 (2008).
48. P. G. Debenedetti, V. S. Raghavan and S. S. Borick, *J. Chem. Phys.* **95**, 4540 (1991).
49. H. E. Stanley, S. V. Buldyrev, M. Canpolat, M. Meyer, O. Mishima, M. R. Sadr-Lahijany, A. Scala and F. W. Starr, *Physica A* **257**, 213 (1998).
50. H. E. Stanley, *Pramana* **53**, 53 (1999).
51. H. E. Stanley, S. V. Buldyrev, M. Canpolat, O. Mishima, M. R. S. A. Sadr-Lahijany and F. W. Starr, *Phys. Chem. Chem. Phys.* **2**, 1551 (2000).
52. M. S. Shell, P. G. Debenedetti and A. Z. Panagiotopoulos, *Phys. Rev. E* **66**, 011202 (2002).
53. J. E. Errington, P. G. Debenedetti and S. Torquato, *J. Chem. Phys.* **118**, 2256 (2003).